Purinergic Signalling (2016) 12:221–233
DOI 10.1007/s11302-016-9496-5

ORIGINAL ARTICLE

Inter-subunit disulfide locking of the human P2X3 receptor elucidates ectodomain movements associated with channel gating

Gabriele Stephan [1] · Maria Kowalski-Jahn [1] · Christopher Zens [1] · Günther Schmalzing [2] · Peter Illes [1] · Ralf Hausmann [2]

Received: 18 November 2015 / Accepted: 19 January 2016 / Published online: 29 January 2016

Abstract P2X3 receptors (P2X3R) are trimeric ATP-gated cation channels involved in sensory neurotransmission and inflammatory pain. We used homology modeling and molecular dynamic simulations of the hP2X3R to identify inter-subunit interactions of residues that are instrumental to elucidate conformational changes associated with gating of the hPX3R. We identified an ionic interaction between E112 and R198 of the head domain and dorsal fin domain, respectively, and E57 and T263 of the lower body domains of adjacent subunits and detected a marked rearrangement of these domains during gating of the hP3X3R. Double-mutant cycle analysis of the inter-subunit residue pairs E112/R198 and E57/T263 revealed significant interaction-free energies. Disulfide locking of the hP2X3R E112C/R198C or the E57C/T263C double cysteine mutants markedly reduced the ATP-induced current responses. The decreased current amplitude following inter-subunit disulfide cross-linking indicates that disulfide locking of the head and dorsal fin domains or at the level of the lower body domains of the hP2X3R prevents the gating-induced conformational rearrangement of the subunits with respect to each other. The distinct reorganization of the subunit interfaces during gating of the hP2X3R is generally consistent with the gating mechanism of other P2XRs. Charge-reversal mutagenesis and methanethiosulfonate (MTS)-modification of substituted cysteines demonstrated that E112 and R198 interact electrostatically. Both disulfide locking and salt bridge breaking of the E112/R198 interaction reduced the hP2X3R function. We conclude that the inter-subunit salt bridge between E112 and R198 of the head and dorsal fin domains, respectively, serves to control the mobility of these domains during agonist-activation of the hP2X3R.

Keywords P2X3 receptor · ATP · Gating · Disulfide trapping

Introduction

P2X receptors (P2XRs) are homo- or heterotrimeric ATP-gated cation channels that assemble from seven homologous subunits referred to as P2X1–P2X7 [1–3]. The application of the apo-closed and the ATP-bound open-state x-ray crystal structures of the zebrafish P2X4 (zP2X4) receptor [4, 5] has facilitated the interpretation of molecular data in a structural context and thus immensely enhanced our understanding of the molecular mechanisms of operation of P2X receptor channels. The zP2X4 protomer has a "jumping-dolphin"-like structural shape with the inter-subunit ATP-binding pocket formed by the head domain, the upper body, and the left flipper of one subunit and the lower body and dorsal fin of an adjacent subunit [5]. The process of ATP activation of P2X receptors comprises several conformational changes throughout the receptor that eventually result in the opening of the transmembrane ion channel pore. Following ATP binding, the head domain and dorsal fin of adjacent subunits approach each other resulting in the tightening of the ATP-binding

Peter Illes and Ralf Hausmann contributed equally to this work.

Electronic supplementary material The online version of this article (doi:10.1007/s11302-016-9496-5) contains supplementary material, which is available to authorized users.

✉ Peter Illes
Peter.Illes@medizin.uni-leipzig.de

✉ Ralf Hausmann
rhausmann@ukaachen.de

[1] Rudolf Boehm Institute of Pharmacology and Toxicology, University of Leipzig, Haertelstrasse 16-18, 04107 Leipzig, Germany

[2] Department of Molecular Pharmacology, RWTH Aachen University, Wendlingweg 2, 52074 Aachen, Germany

pocket [6]. The importance of the movement of the head domain for the ATP activation of P2XRs is also evident from voltage-clamp fluorometry experiments of the P2X1R [7] as well as molecular dynamic simulations (MDS) and normal mode analysis of the P2X4R [8]. The upward and outward movements of the dorsal fin and left flipper, respectively, promote the outward flexing of the lower body domains, which separates the β strands of adjacent subunits and ultimately opens the ion channel pore by an iris-like widening of the TM helices [4]. Taken together, during channel gating, extensive rearrangements and conformational changes take place at the subunit interface (for review, see [9–11]).

In accordance with this gating mechanism, several mutational studies on P2X1 or P2X2 subunit-containing receptors have shown that the restriction of the relative movements of adjacent subunits by disulfide locking inhibits the channel function [12–20]. In the hP2X3R, we have recently shown by disulfide trapping analysis that the conformational mobility of domains constituting the inter-subunit ATP-binding site is essential for ATP-induced channel opening [21]. By using homology modeling and functional analysis of alanine mutants, the residues K63, K65, T172, K176, N279, F280, R281, and K299 of the hP2X3R were identified to be important for ATP-binding [22].

The rapid desensitization of the P2X3R, together with its sensitivity to extracellular Ca^{2+} that accelerates recovery from desensitization makes them unique among P2XRs [23]. Interestingly, it was shown that alanine replacement of the rP2X3R residue E111 of the E111–E112 sequence specific for the rat and human P2X3R accelerated recovery from desensitization but maintained the Ca^{2+} sensitivity of recovery from desensitization [24]. However, although several residues and domains that control desensitization of the P2X3R have been identified [3, 11, 23, 25], the precise molecular mechanism of desensitization remains unknown.

P2X3Rs are crucially involved in sensory neurotransmission and neuropathic and chronic inflammatory pain states [26, 27]. Several compounds pharmacologically targeting P2X3Rs have been developed and exhibited strong antinociceptive effects in rodents [28]. The P2X3 and P2X2/3 antagonist AF-219 was recently shown to be highly effective in reducing the frequency of cough in a phase 2 trial of patients with refractory chronic cough [29]. Antagonists of P2X3-containing receptors such as AF-219 also hold promise for the treatment of lower urinary tract dysfunctions [30].

In a preceding paper, we simulated molecular dynamics of the hP2X3R, based upon its closed homology model, and thereby identified regions of the receptor ectodomain approaching each other around the agonist binding pocket [21]. Then, we generated potential cysteine double mutants in order to check the possibility of disulfide bond formation and subsequent immobilization/inactivation of the receptor. In the present study, we pursued a somewhat different strategy. We searched, based on the homology model of the hP2X3R, by the use of adequate software for potential hydrogen bonds and salt bridges within the receptor structure. Then, cysteine double mutants helped to identify a functionally important interaction between the residues E112 of the head domain of one subunit and the R198 of the dorsal fin of the adjacent subunit, and also another hitherto unknown interaction between the residues E57 and T263 at the lower body domains of adjacent subunits. In addition, charge reversal mutagenesis and methanethiosulfonate-modification of substituted cysteines demonstrated that the negatively charged residue E112 and the positively charged residue R198 interact electrostatically.

Material and methods

Homology modeling of the hP2X3R and MDSs

The apo closed-state and ATP-bound open-state models of the hP2X3 were generated by the Modeller 9v8 program (http://salilab.org/modeller) using the pdb entries 3H9V [5] and 4DW1 [4], respectively, as previously described [21, 31]. To determine the probability of electrostatic or hydrogen bond interactions of amino acid residues of the hP2X3 closed state throughout the protein dynamics in absence of the agonist, we simulated molecular dynamics with NAMD [32] (http://www.ks.uiuc.edu/Research/namd) based on the closed-state hP2X3 homology model, visualized the receptor structure and dynamics with visual molecular dynamics (VMD) [33] (http://www.ks.uiuc.edu/Research/vmd) and used the Salt Bridges plugin (version 1.1) or HBonds plugin (version 1.2) of VMD, respectively, with default settings for the prediction of salt bridges or hydrogen bond interactions throughout the MD trajectories. Only salt bridges or hydrogen bond interactions with a frequency of occupancy of >27 or >50 %, respectively, were analyzed further. Distances between the predicted interacting residues were measured between the respective backbone C_α atoms or the charged or polar atoms of the side chains in the apo closed-state and ATP-bound open-state models of the hP2X3R.

Site-directed mutagenesis

The pIRES2-EGFP plasmid carrying the hP2X3R gene was available from previous studies [22, 34]. All mutants of the hP2X3R were generated by using the QuikChange site-directed mutagenesis kit (Stratagene, La Jolla, CA), using primers synthesized by MWG Biotech (Ebersberg, Germany). All constructs were verified by nucleotide sequencing.

Culturing of HEK293 cells and transient transfection

Human embryonic kidney 293 (HEK293) cells were cultured in Dulbecco's modified Eagle's medium (DMEM) supplemented with 4.5 mg/ml of D-glucose, 10 % of fetal bovine serum (Invitrogen), and 2 mM L-glutamine (Sigma-Aldrich) at 37 °C and 5 % CO_2 in humidified air. For patch clamp electrophysiology, HEK293 cells were plated in plastic dishes 6 h before transient transfection. Following the manufacturer's protocol, 0.5 μg plasmid DNA was mixed with 10 μl of PolyFect® transfection reagent (QIAGEN) and 100 μl of Opti-MEM® (Invitrogen) and was added to the HEK293 cells in culture medium. About 18 h post-transfection, the medium was replaced by Opti-MEM for removing residual plasmid DNA.

Whole-cell patch clamp recordings

Whole-cell patch clamp recordings were performed at room temperature (20–22 °C) 2–4 days after transient transfection of HEK293 cells, using an Axopatch 200 B patch clamp amplifier (Molecular Devices). The pipette solution contained (in mM) CsCl 135, $MgCl_2$ 2, HEPES 20, EGTA 11, $CaCl_2$ 1, Mg-ATP 1.5, and Li-GTP 0.3; pH adjusted to 7.4 using CsOH. The external physiological solution contained (in mM) NaCl 135, KCl 5, $MgCl_2$ 2, $CaCl_2$ 2, HEPES 10, and glucose 11; pH adjusted to 7.4 using NaOH. The pipette resistances were between 3 and 7 MΩ. The liquid junction potential (V_{LJ}) between the bath and pipette solution at 21 °C was calculated to be −4.5 mV. Holding potential values given in this study were corrected for V_{LJ}. All the recordings were carried out at a holding potential of −65 mV. Data were filtered at 2 kHz, digitized at 5 kHz, and stored on a computer using a Digidata 1440 interface and the pClamp 10.2 software (Molecular Devices).

Drugs were dissolved in the external solution and locally superfused to single cells using the SF-77B Perfusion Fast-Step rapid solution exchange system (Warner Instruments). The hP2X3Rs were activated by applying incrementally increasing concentrations (0.3 to 300 μM) of the P2X1R, P2X3R-selective agonist α,β-methylene ATP (α,β-meATP) for 2 s at an interval of 5 min. The amplitudes of the agonist-induced currents were plotted as concentration-response curves as detailed in the following section.

For the redox experiments, the reference electrode for voltage recording was connected to the bath solution via a KCl-agar bridge to avoid voltage errors. To indirectly monitor disulfide bond formation in the redox experiments, 30 μM α,β-meATP was repetitively applied for 2 s at an interval of 5 min, eight times in total. After 10 min (i.e., following two agonist applications), 1 mM dithiothreitol (DTT) was superfused for 15 min (during three agonist applications), followed by the application of 2 mM H_2O_2 for 15 min (during three agonist applications) to initiate and reduce disulfide bonds, respectively. To determine the effect of the methanethiosulfonate (MTS) reagents, the HEK293 cells expressing the wild-type (wt) or mutant hP2X3R were incubated in 1 mM of the respective MTS reagent for 5 min, before incrementally increasing concentrations of α,β-meATP (0.3 to 300 μM) were applied to generate concentration response curves.

Data analysis

The agonist concentration-response curves were obtained by fitting the three-parametric Hill equation $I = I_{max} \cdot [A]^{n_H} / (EC_{50}{}^{n_H} + [A]^{n_H})$ to the pooled data points (unless otherwise stated) from several (n) cells using the Origin 8.0 software (OriginLab), where I is the defined as peak current evoked by α,β-meATP concentration [A], I_{max} is the peak current evoked by a maximally effective α,β-meATP concentration, EC_{50} is the half-maximal effective concentration, and n_H is the Hill coefficient. The data are presented as the means ± S.E.M. of n experiments.

The relative current response elicited by 30 μM α,β-meATP during DTT or H_2O_2 application mediated by the wt hP2X3R and the various hP2X3R mutants was calculated as follows: $(I_{after}/I_{initial}) \times 100$, where $I_{initial}$ and I_{after} are the averaged α,β-meATP current amplitudes measured initially in extracellular solution (EC) and the third α,β-meATP current amplitude after starting the indicated treatment, respectively. For a statistical comparison of the α,β-meATP-elicited current responses of the cysteine and charge scan mutants as well as the effect of the MTS treatment with the wt hP2X3R, a one-way analysis of variance (ANOVA) was used followed by the Holm-Sidak post hoc test. The effect of DTT and H_2O_2 was statistically evaluated by ANOVA followed by the Bonferroni post hoc multiple comparison test. A p value of ≤0.05 was considered statistically significant.

For double mutant cycle analysis, the change in the Gibbs free energy ($\Delta\Delta G$) and the interaction free energy (also designated as the coupling energy of the interaction of two residues, $\Delta\Delta G_{INT}$) were calculated as previously described by using experimentally determined EC_{50} values [35].

Results

Homology modeling predicts inter-subunit interactions of the ectodomain interfaces that rearrange during gating of the hP2X3R

To identify functionally important inter-subunit interactions of the hP2X3R ectodomain that undergo conformational rearrangement during channel gating, we compared the apo closed-state and ATP-bound open-state homology models of

the hP2X3R (Fig. 1a, c). The exclusive comparison of the static apo closed-state and ATP-bound open-state homology models do not allow to assess whether putative side chain interactions of nearby residues are stable during the protein dynamics in each conformational state. To take account of this fact, we performed MDS to determine the probability of the electrostatic or hydrogen bond interactions of amino acid residues of the hP2X3 throughout the closed-state protein dynamics. The comparison of the closed-state and open-state homology models of the hP2X3R indicated a marked rearrangement of the head and dorsal fin domains and the lower body domains. At the lower body domains, our analysis predicted that the side-chains of the residues K242 and T263 (but not R264) of one subunit are in closer proximity to E57 of the adjacent subunit in the closed-state than in the open-state (Fig. 1b, d; Suppl. Table S1). The MDS data further inferred a frequency of occupancy of inter-subunit hydrogen bonding interactions between E57 and either K242 or T263 of 72.8 or 55.6 %, respectively, during the closed state dynamics. At the level of the ATP-binding pocket, the comparison of the closed-and open-state homology models predicted a closer side-chain proximity (distance of the charged atoms) of E112 of the head domain (corresponding to residues Q104–C153) of one subunit and R198 of the dorsal fin (corresponding to residues L191–L216) of the adjacent subunit in the open state than in the closed state (Fig. 1b, d; Suppl. Table S1). In agreement with the closer proximity of the side chains of the residues E112 and R198 in the ATP-bound open state, MDS revealed a frequency of occupancy of this salt bridge interaction of only 27.6 % during the closed-state dynamics.

In addition, our MDS data revealed an inter-subunit hydrogen bond interaction between D79 and Y285 of the upper body domains of adjacent subunits with a frequency of occupancy of 60.5 % during the closed state dynamics of the hP2X3R (Fig. 1b, d; Suppl. Table S1). In this case, the

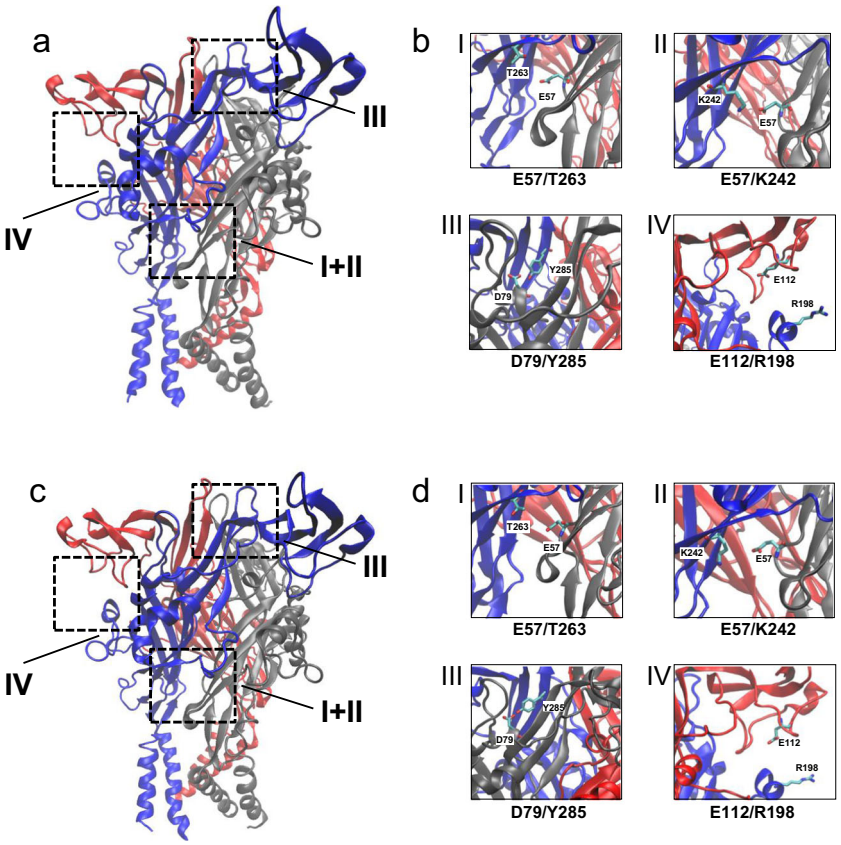

Fig. 1 Homology modeling of the hP2X3 receptor assigns putative inter-subunit interactions. **a**, **b** Shown are ribbon representations of homology models of the hP2X3R in the apo closed-state (**a**) and ATP-bound open-state (**c**). The models are based on the closed-state and ATP-bound open-state crystal structure of the zebrafish zP2X4R, respectively. The three subunits are colored *blue*, *red*, or *gray*. Each subunit has a dolphin-like structure, consisting of the beak, the head, upper- and lower body domains, the dorsal fin, and left and right flippers (c.f. [5]). **b**, **d** Comparison of the closed-state (**b**) and ATP-bound open-state (**d**) hP2X3 homology models and refinements by molecular dynamics simulations led to the identification of the following four residue pairs possibly involved in non-covalent inter-subunit interactions: the hydrogen-bonded pairs E57/T263 and D79/Y285 located at the lower and the upper body domains, respectively; the electrostatically linked pairs E57/K242 and E112/R198 located at the lower body domains and the head and the dorsal fin domains of two adjacent subunits, respectively. The side chains of the putatively interacting residues of each residue pair are shown as cyan sticks with oxygens and nitrogens highlighted in *red* or *blue*, respectively. The backbone colors allow distinguishing the subunits as in panels **a** and **c**

polar/charged atoms were separated by a distance of about 3 Å in the closed state only and did not approach each other in the ATP-bound open state of the receptor.

Disulfide locking of inter-subunit residue pairs E57C/T263C and E112C/R198C blocks hP2X3R channel function

To test for their spatial proximity at the subunit interface, we singly and doubly substituted the MDS-predicted residues by cysteines for oxidative cross-linking experiments. To analyze the effect of the cysteine substitution itself, current responses to the P2X1R/P2X3R-selective agonist α,β-meATP (0.3–300 μM) were recorded by whole-cell patch clamping from HEK293 cells transiently expressing the wt hP2X3 receptor or one of its single or double cysteine mutants. Double cysteine substitution markedly reduced the maximal current amplitude (efficacy) elicited by α,β-meATP at the E57C/T263C or the E112C/R198C mutant (Fig. 2a, d; Table 1). The current responses of the E57C/K242C and the D79C/Y285C mutants were virtually abolished (Fig. 2b, c; Table 1). Because the single cysteine mutant D79C was also virtually non-functional, the abolished function of the cysteine double mutant D79C/Y285C most likely can be attributed to the cysteine substitution of the residue D79. The half maximal effective concentration (EC_{50}) of α,β-meATP, the mean current amplitude elicited by 300 μM of α,β-meATP (I_{mean}), and the Hill coefficient (n_H) of each hP2X3R mutant are summarized in Table 1.

Next, we analyzed whether the current amplitudes induced by 30 μM α,β-meATP were affected by chemical reduction or oxidation by 1 mM DTT or 2 mM H_2O_2 treatment as an indicator of the cleavage and re-formation of a disulfide bond, respectively. As shown in Fig. 3, DTT or H_2O_2 treatment did not significantly affect the current amplitudes mediated by the wt hP2X3R, its single cysteine mutants (with the exception of a small change at E112C) or the E57C/K242C and the D79C/Y285C cysteine double mutants (Fig. 3 a–c). Both double-cysteine mutants, E57C/K242C and the D79C/Y285C, turned out to be virtually non-functional even in the presence of high concentrations of DTT (c.f. Fig. 2b, c and Fig. 3a). Therefore, we cannot assess whether disulfide bonds are formed between the E57C and K242C or the D79C

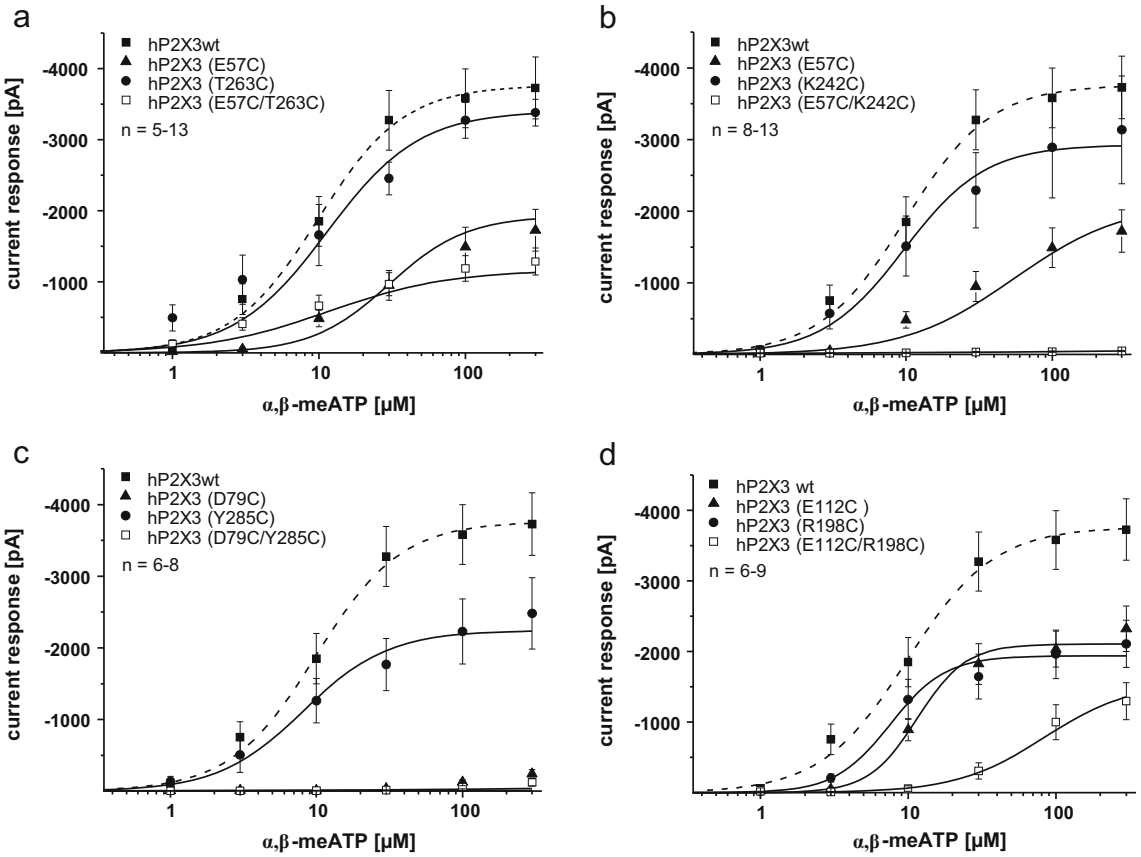

Fig. 2 α,β-meATP dose–response curves of the cysteine substitution mutants of the predicted interacting residues of the hP2X3R subunit interfaces. α,β-meATP induced current responses were recorded from HEK293 cells transfected with the wt hP2X3R or one of its single or double cysteine mutants as indicated. Increasing concentrations of α,β-meATP (0.3–300 μM) were applied locally for 2 s in 5-min intervals at a holding potential of −65 mV. Each *symbol* represents the mean ± SEM of 6–15 experiments. The *continuous and broken lines through symbols* are fits to the Hill equation. The relevant parameters derived from these curves are summarized in Table 1

Table 1 Summary of the data obtained from concentration-response analysis of the wt hP2X3R and its single and double mutants

	EC_{50} [μM]	n_H	I_{mean} [pA] 300 μM	$\Delta\Delta G$ [kcal/mol]	$\Delta\Delta G_{INT}$ [kcal/mol]	Number
hP2X3 wt	9.86 ± 3.11	1.49 ± 0.2	−3727.92 ± 434.81	0	–	8
E57C[c]	30.08 ± 5.35	1.64 ± 0.2	−1724.40 ± 295.46[a]	0.65 ± 0.011	–	13
T263C[c]	11.35 ± 4.36	1.38 ± 0.3	−3380.86 ± 190.17	0.08 ± 0.001	–	6
E57C/T263C[c]	11.66 ± 5.18	1.06 ± 0.1	−1285.88 ± 191.72[a]	0.10 ± 0.006	−0.63 ± 0.20	5
K242C	9.65 ± 1.90	1.55 ± 0.1	−3136.92 ± 751.77	−0.01 ± 0.003	–	13
E57C/K242C	n.c.	n.c.	−49.09 ± 9.77[a]	n.c.	n.c.	10
D79C	n.c.	n.c.	−242.09 ± 57.52[a]	n.c.	–	7
Y285C	8.14 ± 1.72	1.49 ± 0.1	−2482.51 ± 497.22	−0.11 ± 0.003	–	7
D79C/Y285C	n.c.	n.c.	−122,41 ± 50.57[a]	n.c.	n.c.	6
E112C	11.51 ± 1.91	2.63 ± 0.5	−2323.90 ± 324.74	0.09 ± 0.04	–	8
R198C	7.56 ± 1.68	2.31 ± 0.3	−2107.14 ± 333.94	−0.15 ± 0.003	–	9
E112C/R198C	83.41 ± 84.76	1.46 ± 0.4	−1297.54 ± 263.66[a]	1.24 ± 0.09	1.31 ± 0.54	6
E112K	46.41 ± 22.06	0.88 ± 0.1	−2200.76 ± 397.17[b]	0.90 ± 0.03	–	6
R198D	56.34 ± 23.72	1.30 ± 0.1	−2989.79 ± 337.52	1.01 ± 0.03	–	8
E112K/R189D	20.08 ± 6.16	1.50 ± 0.2	−3719.87 ± 356.08	0.45 ± 0.01	−1.50 ± 0.01	8

Half maximal effective concentration (EC_{50}), Hill coefficient (n_H), mean current amplitudes elicited by 300 μM α,β-meATP (I_{mean}), ΔΔG and $\Delta\Delta G_{INT}$ values and the number of measured HEK293 cells expressing the mutant or wt hP2X3 receptor (*n*) are summarized. Values represent mean ± S.E.M

n.c. non-calculable

[a] I_{mean} values at 300 μM α,β-meATP are significantly different from those measured in hP2X3 wt. Statistics were carried out with one-way ANOVA followed by Holm-Sidak post hoc test after confirming normal distribution

[b] I_{mean} values at 300 μM α,β-meATP are significantly different from those measured in hP2X3 wt. Statistics were carried out with Student's *t* test after confirming normal distribution

[c] Because fitting the Hill equation to the pooled data points from (*n*) cells did not reliably characterize the concentration-response relationship of these mutants, the EC_{50} and n_H values were calculated by averaging the EC_{50} and n_H values of a cell-by-cell curve fitting to the Hill equation

and Y285C. It is possible that the disulfide bonds are formed, but adopt a buried position that renders them inaccessible to DTT treatment. Alternatively, the single cysteine substitution of D79 or the simultaneous cysteine substitution of E57 and K242 may profoundly disturb the synthesis, assembly, trafficking, or channel function of these mutants. By contrast, the α,β-meATP-induced current amplitudes of the cysteine double mutants E57C/T263C and E112C/R198C were significantly increased by chemical reduction with DTT (Fig. 3a, c). This DTT-induced increase of the α,β-meATP-induced current amplitudes could be fully reversed by the subsequent H_2O_2 treatment.

Double mutant cycle analysis supports the pairwise energetic coupling of E57/T263 and E112/R198

To test for energetic coupling between the residue pairs E57/T263 and E112/R198, we performed a double-mutant cycle analysis. The double-mutant cycle analysis allows the calculation of the interaction energy between a residue pair based on the Gibbs free energy change associated with the mutation of these residues [36–40]. If two residues interact, the change in the free energy of the double mutant differs from the sum of the changes of the corresponding single mutations. We used the changes of the EC_{50} values for α,β-meATP to calculate the free energy change associated with the cysteine substitutions E57C/T263C and E112C/R198C. We found for both residue pairs that the additive sum of the changes in the free energy of the single mutants was different from the change in the free energy of the corresponding double mutant. Interaction energies of ($\Delta\Delta G_{INT}$) −0.63 ± 0.20 and 1.31 ± 0.54 kcal/mol were calculated for the residue pairs E57C/T263C and E112C/R198C, respectively (Fig. 4 and Table 1). Both interaction energies are significantly larger than the threshold value set to ±0.35 kcal/mol for non-interacting residues [35, 36]. In addition, mutant cycle analysis for the charge reversal mutants E112K and/or R198D provided an interaction free energy ($\Delta\Delta G_{INT}$) of −1.50 ± 0.01 kcal/mol (Table 1), which is also above the threshold of ±0.35 kcal/mol for non-interacting residues [36]. However, one should consider that mutant cycle analysis based on EC_{50} values can merely estimate the energetics of the interaction, because EC_{50} values represent a composite measure of agonist binding, channel gating, and desensitization and each mutation may differently affect these individual processes during channel activation.

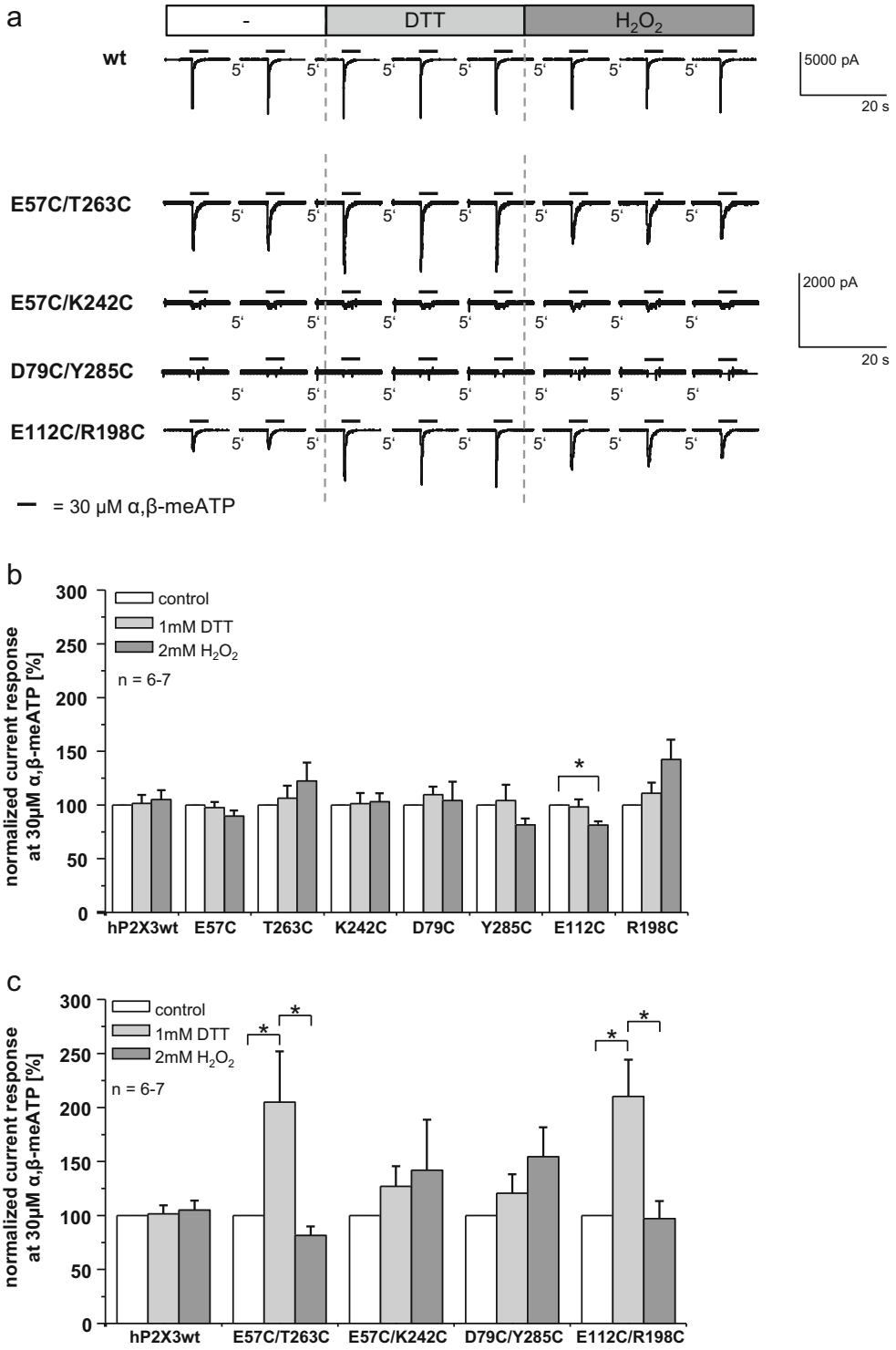

Fig. 3 Analysis of the predicted interacting residue pairs of the hP2X3R by disulfide trapping. **a** Original current traces as recorded by whole cell patch-clamping of HEK293 cells expressing the indicated hP2X3R. Current responses were elicited by 30 μM α,β-meATP applied repeatedly for 2 s in 5-min intervals before, during and after treatment with 1 mM DTT or 2 mM H_2O_2 as indicated. **b**, **c** The mean current responses recorded as in (**a**) of the wt hP2X3 and hP2X3R single (**b**) or double (**c**) cysteine mutants during treatment with DTT or H_2O_2 were normalized to the current responses prior to DTT/H_2O_2 treatment. Each *bar* represents mean ± SEM of 6–7 experiments. Statistics were carried out with one-way ANOVA followed by the Bonferroni post hoc test (*$p < 0.05$)

The E112/R198 interaction is electrostatic in nature

Next, we analyzed whether the interaction between E112 and R198 of the hP2X3 receptor is electrostatic in nature. We individually reversed the charges and swapped the charges to break and restore the ionic interactions, respectively. Because the current responses of the charge reversal mutants did not reliably saturate at the largest α,β-meATP concentration used, the curve fitting with the Hill equation may report only an estimate of the top of

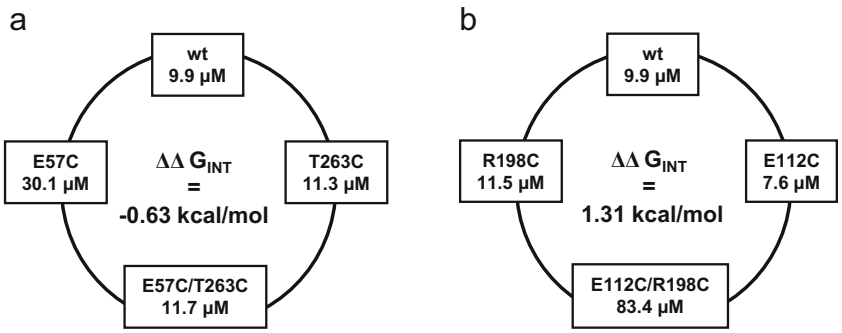

Fig. 4 EC_{50} value-based double mutant cycle analysis of hP2X3 cysteine single and double mutants to assess the energetic coupling of E57/T263 and E112/R198. The α,β-meATP EC_{50} values of the indicated hP2X3R constructs were derived from the dose–response curves (see Table 1). The indicated interaction free energies of both residue pairs, E57/T263 and E112/R198, are significantly larger than the threshold, set to ±0.35 kcal/mol for non-interacting residues [36]. For details of the free energy calculations, see [35]

the concentration-response curve. Thus, we decided to use the maximal current amplitudes elicited by the largest α,β-meATP concentration used (300 μM; I_{mean}) for the comparison of I_{max} values between the wt and its mutants rather than the estimated top of the concentration-response curves obtained from the fitting with the Hill equation. Our reason for not increasing the α,β-meATP concentration above 300 μM was that we were afraid of inducing non-selective effects at overtly large agonist concentrations (e.g., long-lasting blockade of ecto-nucleotidases with subsequent marked desensitization of the P2X3 receptor due to the reduced degradation of released endogenous ATP; [41]).

In the charge reversal studies, we used lysine (E112K) or aspartic aid (R198D) for substitution. At first, we compared the I_{mean} values after charge reversal and charge swap in the hP2X3R at 30 μM α,β-meATP (Fig. 5c). The E112K and R198D single mutations both depressed the current responses, whereas the E112K/R198D double mutation reversed this inhibitory effect. We carried out a more detailed analysis at 300 μM α,β-meATP (Fig. 5d), because all residual calculations were made at this agonist concentration (Table 1). In this case, only the E112K single mutation of wt hP2X3 inhibited the current responses and the R198D single and the E112K/R198D double mutations failed to cause any statistically significant change. If we disregarded statistical significance and calculated the tendency of changes in agonist potency and mean current amplitude elicited by 300 μM α,β-meATP, the charge reversal resulted in a 4.7- or 5.7-fold decrease of the α,β-meATP potency, respectively, and a 1.7- or 1.3-fold decrease of the maximal current amplitude elicited by 300 μM α,β-meATP, respectively, compared with the wt hP2X3 receptor (Table 1 and Fig. 5a, b).

If the effects of the charge reversal mutations E112K and R198D occur independent of each other, the effect of the double charge reversal should be equal to the product of the two individual changes, i.e., a total ~27-fold decrease in the α,β-meATP potency and a total ~2-fold decrease in the maximal current amplitude would be expected. In contrast, the charge-swap mutant E112K/R198D of the hP2X3R exhibited only a twofold decrease in the potency and no change of the maximal current amplitude elicited by 300 μM α,β-meATP compared with the wt hP2X3R (Table 1, Fig. 5b, c). This indicates that the charge swapping of the E112/R198 residue pair largely rescues the α,β-meATP potency and the maximal current amplitude elicited by 300 μM α,β-meATP and thus suggests that the effects of the charge reversal mutations in the E112K/R198D charge-swap mutant occur not independent (non-additive) of each other.

To provide additional evidence for the electrostatic nature of the interaction between E112 and R198, we used the single cysteine substitution mutants E112C and R198C to posttranslationally add charges to the 112C and 198C by cysteine-reactive MTS reagents. The E112C or R198C single mutations themselves did not significantly affect the α,β-meATP potency (Fig. 2d, Table 1), but decreased the maximal current amplitude elicited by 300 μM α,β-meATP by the factor of 1.8 or 2, respectively (Fig. 2d, Table 1). To reintroduce desired charges at positions 112 and 198 posttranslationally, we used the positively and negatively charged MTS reagents MTS ethylammonium (MTSEA) and MTS ethylsulfonate (MTSES), respectively. According to the similar molecular mass and thiol reactivity of these two MTS reagents, the differences in the α,β-meATP potency and maximal current amplitudes following treatment with MTSEA or MTSES can be ascribed to the addition of a positive or negative charge at the substituted cysteine, respectively. Treatment of the wt hP2X3R with 1 mM MTSEA or MTSES for 5 min failed to affect either the current amplitudes elicited by 300 μM α,β-meATP (Fig. 6a, d) or its potency (Fig. 6a). The restoration of the original charges at E112C or R198C by MTSES or MTSEA (which itself did not induce any currents), respectively, rescued the

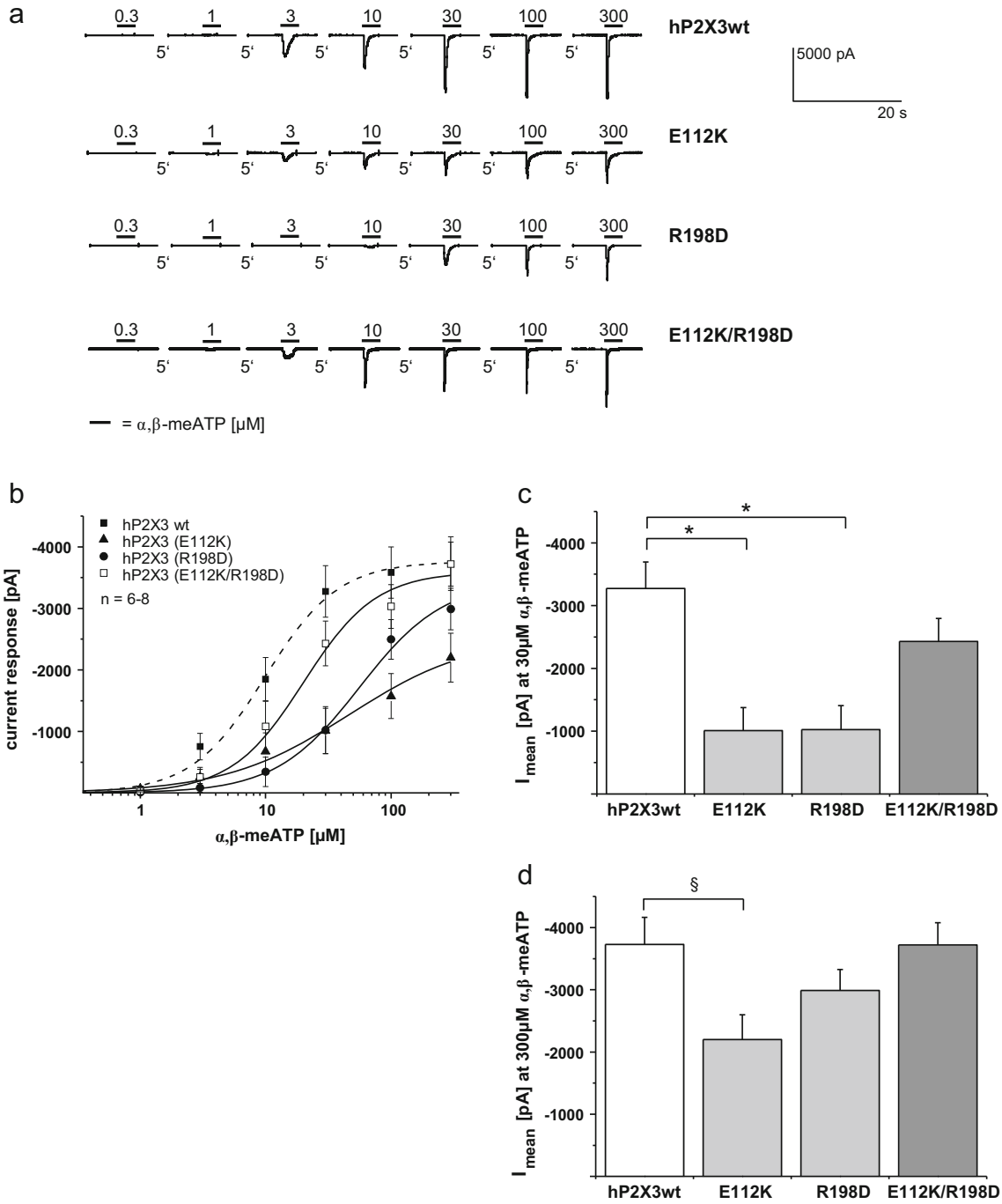

Fig. 5 Analysis of the E112/R198 residue pair by charge reversal and charge swapping mutagenesis to assess whether E112 and R198 interact electrostatically. **a** Original current responses of HEK293 cells expressing the indicated hP2X3R constructs to increasing concentrations of α,β-meATP (*horizontal bars*, concentration in μM) applied for 2 s in 5-min intervals. **b** α,β-meATP dose–response curves of the wt hP2X3R or the E112K, R198D or E112K/R198D mutant of the hP2X3R were derived from measurements such shown in panel **a**. Mean current responses to 30 μM α,β-meATP (**c**) or 300 μM α,β-meATP (**d**) of the wt hP2X3R or the E112K, R198D or E112K/R198D mutant of the wt hP2X3R. Each *bar* represents mean ± SEM of 6–8 experiments. Statistics were carried out with one-way ANOVA followed by Holm-Sidak post hoc test (*$<p<0.05$) or by the Student's *t* test after confirming normal distribution ($^{\S}p<0.05$)

receptor function as evident from the increase of the α,β-meATP-induced current amplitudes to approximately the same values as of the wt hP2X3R (Fig. 6b–d). By contrast, the introduction of a charge opposite to the original one at each position did not markedly affect the function of the E112C- or R198C-hP2X3R (Fig. 6b–d).

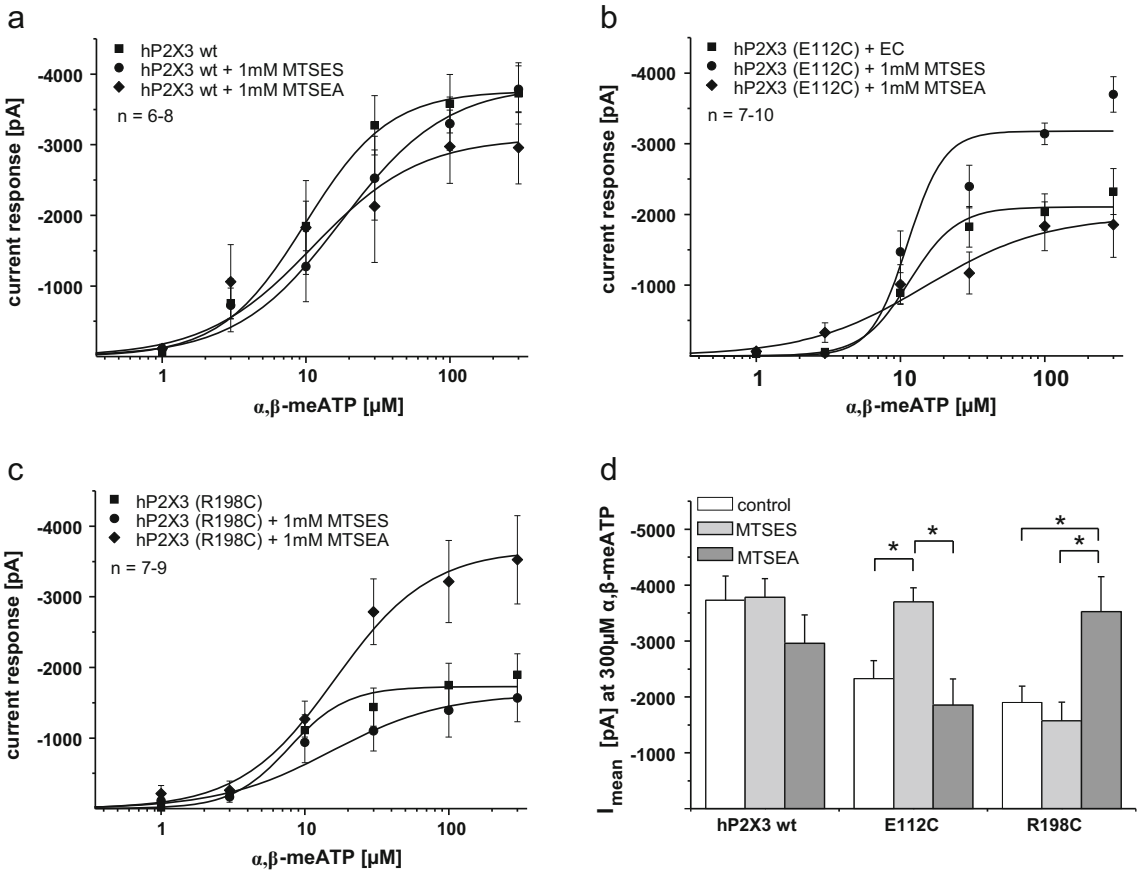

Fig. 6 Analysis of the E112C or R198C residues by cysteine modification via the thiol-reactive MTS reagents MTSES or MTSEA. α,β-meATP dose–response curves were generated as described in the legend of Fig. 2 at HEK293 cells transfected with the wt hP2X3R (**a**), the E112C-hP2X3R (**b**), and the R198C-hP2X3R (**c**). Prior to whole-cell patch clamp analysis, the cells were pre-incubated in extracellular solution without or with 1 mM MTSES (negatively charged) or 1 mM MTSEA (positively charged) as indicated. **d** *Bars* represent mean current responses ± SEM of 6–10 experiments to 300 μM α,β-meATP of the indicated hP2X3R constructs pre-incubated in extracellular solution without (control) or with MTSES or MTSEA as indicated. Statistics were carried out with one-way ANOVA followed by Holm-Sidak post hoc test (*$p < 0.05$)

Discussion

In this study, we have identified functionally important inter-subunit interactions of the hP2X3 receptor that were instrumental to elucidate conformational changes associated with ATP-induced gating. Homology modeling and MDS revealed a marked rearrangement of the head and dorsal fin domains and the lower body domains of adjacent subunits during channel gating of the hP3X3R. These findings closely agree with the described ATP-induced tightening of the ATP-binding jaw (also designated cleft closure) between the head and dorsal fin domains [4, 6] and the separation of the lower body domains of adjacent subunits of the P2X2 or P2X4 receptor during channel gating [4, 14, 42]. MDS predicted the inter-subunit hydrogen bonding interaction of the lower body residues E57 and either K242 or T263, and between the upper body residues D79/Y285 and the ionic interaction of the residues E112 of the head domain and R198 of the dorsal fin that were experimentally analyzed by disulfide trapping. Unexpectedly, the E57C/K242C and the D79C/Y285C double cysteine mutants were virtually non-functional even in the presence of high concentrations of DTT. By contrast, the α,β-meATP-induced current amplitudes of the cysteine double mutants E57C/T263C and E112C/R198C were significantly affected by chemical reduction or oxidation by DTT or H_2O_2 treatment, respectively. The ability of the E57C/T263C and the E112C/R198C cysteine double mutants to form inter-subunit disulfide bonds confirms that the residues of each pair are in close spatial proximity at the subunit interface. In addition, double-mutant cycle analysis of the inter-subunit residue pairs E57/T263 and E112/R198 revealed significant interaction free energies, indicating that E57/T263 and E112/R198 are pairwise energetically coupled.

The increase of the α,β-meATP-evoked current amplitudes by DTT without prior exposure to H_2O_2 suggests that both hP2X3 cysteine double mutants, E57C/T263C and E112C/R198C, are partially locked in a non-activatable state by disulfide bonds that form spontaneously, i.e., in the absence of

added H_2O_2. Application of H_2O_2 induced the re-formation of an inter-subunit disulfide cross-link between the E57C and T263C or the E112C and R198C residues as indicated by the diminished α,β-meATP-gated currents following H_2O_2 treatment that apparently reflect the locking of both mutants in a less activatable state. Thus, our disulfide trapping experiments are best compatible with the view that inter-subunit disulfide locking of the head and dorsal fin domains or at the level of the lower body domains prevents the gating-induced conformational rearrangement of the subunits with respect to each other. These results are consistent with findings of former studies on P2X1R, P2X1/2R, P2X2R, and P2X4R, which were elaborated by using a similar approach [12, 14–20], reviewed in [9].

An amino acid sequence alignment of the hP2X1, rP2X2, and hP2X3 receptors in combination with our hP2X3R homology model disclosed additional interesting parallels. The residues pairs E112/R198 and E57/T263 of the hP2X3R are located at positions equivalent to residues located at the head and dorsal fin domains of the P2X1R and P2X2R and the functionally important E63/R274 salt bridge of the rP2X2R [14], respectively. In the hP2X1R or rP2X2R, restriction by disulfide crosslinking of the movement of the head domain relative to the adjacent subunit [16] or dorsal fin [19], respectively, also markedly reduced the ATP-elicited current responses (for review, see [9]). Likewise, disulfide crosslinking of the E63C/R274C residue pair at the lower body interface of the rP2X2R significantly reduced the ATP-induced current amplitudes [14]. These findings indicate that the agonist-induced inter-subunit conformational changes in the hP2X3R are similar to those in the hP2X1R or rP2X2R and suggest that the principal conformational changes associated with channel opening of the hP2X3 receptor are the movement of adjacent subunits relative to each other. The marked reorganization of the interfaces between subunits during gating of P2X receptors [4, 9] parallels the gating mechanism of pentameric ligand-gated ion channels [43, 44].

Charge-reversal and charge-swap mutagenesis and MTS-modification of substituted cysteines provides experimental evidence that E112 and R198 interact electrostatically. Moreover, several lines of evidence suggest that the salt bridge between E112 and R198 serves to control the mobility of the head domain of one subunit relative to the dorsal fin domain of the adjacent subunit: First, disruption of the ionic interaction between E112 and R198 by a single cysteine substitution or single charge reversal mutagenesis (but not charge swapping) markedly reduced the α,β-meATP-induced current amplitude or reduced both the maximal current amplitude and the α,β-meATP potency, respectively. These results suggest that the unrestricted mobility of the head and dorsal fin domains due to the loss of the ionic interaction between E112/R198 impedes the hP2X3R function, most likely by affecting channel gating. Second, conformational fixation of the head and dorsal fin domains of adjacent subunits by a disulfide lock diminished the agonist-induced current amplitudes by inhibiting the gating-dependent conformational changes rather than agonist binding (present study and see [21]). There is also evidence from the literature that the conformational mobility of the head domain relative to the adjacent subunit of the P2XRs is essential for channel gating [6–8, 16, 21]. The observations that both conformational restriction (by disulfide locking) and mobility (by salt bridge breaking) are detrimental for function seems, at the first glance, contradictory. However, due to a higher conformational degree of freedom with respect to the spatial orientation of the oppositely charged side chains, salt bridges enable a significant mobility as compared to covalent bonds or other non-bonded interactions such as hydrogen bonds or hydrophobic interactions, while also maintaining a strong interaction. Due to this characteristic, an inter-domain salt bridge is ideally suitable to control the structural dynamics of coupled or interacting protein domains during processes associated with conformational rearrangements such as channel gating (e.g., by switching between distinct "lock states"): On the one hand, a salt bridge constrains the domain flexibility [45–47], but on the other hand, allows a certain degree of reorientation of side chains forming this inter-domain salt bridge. In this regard, salt bridges within or between subunits of ion channels or G protein-coupled receptors have been shown to be critical for state-dependent conformational stability, domain flexibility, and gating (for instance, see [35, 48–51]).

In summary, the present study revealed two main conclusions: First, one principal conformational change associated with channel opening of the hP2X3R are the rearrangements of adjacent subunits relative to each other, which is generally consistent with the gating mechanism of the hP2X1R, rP2X2R, or zP2X4R. Second, the hP2X3R residues E112 and R198 of the head domain and dorsal fin domain, respectively, form an inter-subunit salt bridge that serves to control the mobility of these domains during agonist-activation of the hP2X3R.

Acknowledgments The study was supported by grants of the Deutsche Forschungsgemeinschaft (RI 2092/1-2, IL 20/18-2, HA 6095/1).

References

1. Khakh BS, North RA (2012) Neuromodulation by extracellular ATP and P2X receptors in the CNS. Neuron 76(1):51–69
2. North RA (2002) Molecular physiology of P2X receptors. Physiol Rev 82(4):1013–1067
3. Kaczmarek-Hajek K, Lorinczi E, Hausmann R, Nicke A (2012) Molecular and functional properties of P2X receptors—recent progress and persisting challenges. Purinergic Signal 8(3):375–417
4. Hattori M, Gouaux E (2012) Molecular mechanism of ATP binding and ion channel activation in P2X receptors. Nature 485:207–212

5. Kawate T, Michel JC, Birdsong WT, Gouaux E (2009) Crystal structure of the ATP-gated P2X(4) ion channel in the closed state. Nature 460(7255):592–598
6. Jiang R, Taly A, Lemoine D, Martz A, Cunrath O, Grutter T (2012) Tightening of the ATP-binding sites induces the opening of P2X receptor channels. EMBO J 31:2134–2143
7. Lorinczi E, Bhargava Y, Marino SF, Taly A, Kaczmarek-Hajek K, Barrantes-Freer A, Dutertre S, Grutter T, Rettinger J, Nicke A (2012) Involvement of the cysteine-rich head domain in activation and desensitization of the P2X1 receptor. Proc Natl Acad Sci U S A 109(28):11396–11401
8. Huang LD, Fan YZ, Tian Y, Yang Y, Liu Y, Wang J, Zhao WS, Zhou WC, Cheng XY, Cao P, Lu XY, Yu Y (2014) Inherent dynamics of head domain correlates with ATP-recognition of P2X4 receptors: insights gained from molecular simulations. PLoS One 9(5):e97528
9. Jiang R, Taly A, Grutter T (2013) Moving through the gate in ATP-activated P2X receptors. Trends Biochem Sci 38(1):20–29
10. Chataigneau T, Lemoine D, Grutter T (2013) Exploring the ATP-binding site of P2X receptors. Front Cell Neurosci 7:273
11. Hausmann R, Kless A, Schmalzing G (2015) Key sites for P2X receptor function and multimerization: overview of mutagenesis studies on a structural basis. Curr Med Chem 22(7):799–818
12. Jiang LH, Kim M, Spelta V, Bo X, Surprenant A, North RA (2003) Subunit arrangement in P2X receptors. J Neurosci 23(26):8903–8910
13. Jiang LH, Rassendren F, Spelta V, Surprenant A, North RA (2001) Amino acid residues involved in gating identified in the first membrane-spanning domain of the rat P2X2 receptor. J Biol Chem 276(18):14902–14908
14. Jiang R, Martz A, Gonin S, Taly A, de Carvalho LP, Grutter T (2010) A putative extracellular salt bridge at the subunit interface contributes to the ion channel function of the ATP-gated P2X2 receptor. J Biol Chem 285(21):15805–15815
15. Kawate T, Robertson JL, Li M, Silberberg SD, Swartz KJ (2011) Ion access pathway to the transmembrane pore in P2X receptor channels. J Gen Physiol 137(6):579–590
16. Roberts JA, Allsopp RC, El AS, Vial C, Schmid R, Young MT, Evans RJ (2012) Agonist binding evokes extensive conformational changes in the extracellular domain of the ATP-gated human P2X1 receptor ion channel. Proc Natl Acad Sci U S A 109:4663–4667
17. Marquez-Klaka B, Rettinger J, Bhargava Y, Eisele T, Nicke A (2007) Identification of an intersubunit cross-link between substituted cysteine residues located in the putative ATP binding site of the P2X1 receptor. J Neurosci 27(6):1456–1466
18. Marquez-Klaka B, Rettinger J, Nicke A (2009) Inter-subunit disulfide cross-linking in homomeric and heteromeric P2X receptors. Eur Biophys J 38(3):329–338
19. Nagaya N, Tittle RK, Saar N, Dellal SS, Hume RI (2005) An intersubunit zinc binding site in rat P2X2 receptors. J Biol Chem 280(28):25982–25993
20. Stelmashenko O, Compan V, Browne LE, North RA (2014) Ectodomain movements of an ATP-gated ion channel (P2X2 receptor) probed by disulfide locking. J Biol Chem 289(14):9909–9917
21. Kowalski M, Hausmann R, Dopychai A, Grohmann M, Franke H, Nieber K, Schmalzing G, Illes P, Riedel T (2014) Conformational flexibility of the agonist binding jaw of the human P2X3 receptor is a prerequisite for channel opening. Br J Pharmacol 171(22):5093–5112
22. Bodnar M, Wang H, Riedel T, Hintze S, Kato E, Fallah G, Groger-Arndt H, Giniatullin R, Grohmann M, Hausmann R, Schmalzing G, Illes P, Rubini P (2011) Amino acid residues constituting the agonist binding site of the human P2X3 receptor. J Biol Chem 286(4):2739–2749
23. Giniatullin R, Nistri A (2013) Desensitization properties of P2X3 receptors shaping pain signaling. Front Cell Neurosci 7:245
24. Fabbretti E, Sokolova E, Masten L, D'Arco M, Fabbro A, Nistri A, Giniatullin R (2004) Identification of negative residues in the P2X3 ATP receptor ectodomain as structural determinants for desensitization and the Ca^{2+}-sensing modulatory sites. J Biol Chem 279(51):53109–53115
25. Hausmann R, Bahrenberg G, Kuhlmann D, Schumacher M, Braam U, Bieler D, Schlusche I, Schmalzing G (2014) A hydrophobic residue in position 15 of the rP2X3 receptor slows desensitization and reveals properties beneficial for pharmacological analysis and high-throughput screening. Neuropharmacology 79:603–615
26. Chizh BA, Illes P (2001) P2X receptors and nociception. Pharmacol Rev 53(4):553–568
27. Wirkner K, Sperlagh B, Illes P (2007) P2X3 receptor involvement in pain states. Mol Neurobiol 36(2):165–183
28. North RA, Jarvis MF (2013) P2X receptors as drug targets. Mol Pharmacol 83(4):759–769
29. Abdulqawi R, Dockry R, Holt K, Layton G, McCarthy BG, Ford AP, Smith JA (2015) P2X3 receptor antagonist (AF-219) in refractory chronic cough: a randomised, double-blind, placebo-controlled phase 2 study. Lancet 385(9974):1198–1205
30. Ford AP, Undem BJ (2013) The therapeutic promise of ATP antagonism at P2X3 receptors in respiratory and urological disorders. Front Cell Neurosci 7:267
31. Riedel T, Wiese S, Leichsenring A, Illes P (2012) Effects of nucleotide analogs at the P2X3 receptor and its mutants identify the agonist binding pouch. Mol Pharmacol 82(1):80–89
32. Phillips JC, Braun R, Wang W, Gumbart J, Tajkhorshid E, Villa E, Chipot C, Skeel RD, Kale L, Schulten K (2005) Scalable molecular dynamics with NAMD. J Comput Chem 26(16):1781–1802
33. Humphrey W, Dalke A, Schulten K (1996) VMD: visual molecular dynamics. J Mol Graph 14(1):33–38, 27–38
34. Hausmann R, Bodnar M, Woltersdorf R, Wang H, Fuchs M, Messemer N, Qin Y, Gunther J, Riedel T, Grohmann M, Nieber K, Schmalzing G, Rubini P, Illes P (2012) ATP binding site mutagenesis reveals different subunit stoichiometry of functional P2X2/3 and P2X2/6 receptors. J Biol Chem 287(17):13930–13943
35. Hausmann R, Gunther J, Kless A, Kuhlmann D, Kassack MU, Bahrenberg G, Markwardt F, Schmalzing G (2013) Salt bridge switching from Arg290/Glu167 to Arg290/ATP promotes the closed-to-open transition of the P2X2 receptor. Mol Pharmacol 83(1):73–84
36. Schreiber G, Fersht AR (1995) Energetics of protein-protein interactions: analysis of the Barnase-Barstar interface by single mutations and double mutant cycles. J Mol Biol 248(2):478–486
37. Carter PJ, Winter G, Wilkinson AJ, Fersht AR (1984) The use of double mutants to detect structural changes in the active site of the tyrosyl-tRNA synthetase (Bacillus stearothermophilus). Cell 38(3):835–840
38. Serrano L, Horovitz A, Avron B, Bycroft M, Fersht AR (1990) Estimating the contribution of engineered surface electrostatic interactions to protein stability by using double-mutant cycles. Biochemistry 29(40):9343–9352
39. Hidalgo P, Mackinnon R (1995) Revealing the architecture of a K+ channel pore through mutant cycles with a peptide inhibitor. Science 268:307–310
40. Horovitz A (1996) Double-mutant cycles: a powerful tool for analyzing protein structure and function. Fold Des 1(6):R121–R126
41. Bultmann R, Trendelenburg M, Tuluc F, Wittenburg H, Starke K (1999) Concomitant blockade of P2X-receptors and ecto-nucleotidases by P2-receptor antagonists: functional consequences in rat vas deferens. Naunyn Schmiedebergs Arch Pharmacol 359(4):339–344
42. Du J, Dong H, Zhou HX (2012) Gating mechanism of a P2X4 receptor developed from normal mode analysis and molecular dynamics simulations. Proc Natl Acad Sci U S A 109(11):4140–4145

43. Sauguet L, Shahsavar A, Poitevin F, Huon C, Menny A, Nemecz A, Haouz A, Changeux JP, Corringer PJ, Delarue M (2014) Crystal structures of a pentameric ligand-gated ion channel provide a mechanism for activation. Proc Natl Acad Sci U S A 111(3):966–971
44. Althoff T, Hibbs RE, Banerjee S, Gouaux E (2014) X-ray structures of GluCl in apo states reveal a gating mechanism of Cys-loop receptors. Nature 512(7514):333–337
45. Kumar S, Nussinov R (2002) Close-range electrostatic interactions in proteins. Chembiochem 3(7):604–617
46. Lam SY, Yeung RC, Yu TH, Sze KH, Wong KB (2011) A rigidifying salt-bridge favors the activity of thermophilic enzyme at high temperatures at the expense of low-temperature activity. PLoS Biol 9(3):e1001027
47. Leng Q, MacGregor GG, Dong K, Giebisch G, Hebert SC (2006) Subunit-subunit interactions are critical for proton sensitivity of ROMK: evidence in support of an intermolecular gating mechanism. Proc Natl Acad Sci U S A 103(6):1982–1987
48. Kash TL, Jenkins A, Kelley JC, Trudell JR, Harrison NL (2003) Coupling of agonist binding to channel gating in the $GABA_A$ receptor. Nature 421(6920):272–275
49. Venkatachalan SP, Czajkowski C (2008) A conserved salt bridge critical for $GABA_A$ receptor function and loop C dynamics. Proc Natl Acad Sci U S A 105(36):13604–13609
50. Wang CI, Lewis RJ (2013) Emerging opportunities for allosteric modulation of G-protein coupled receptors. Biochem Pharmacol 85(2):153–162
51. Cui G, Freeman CS, Knotts T, Prince CZ, Kuang C, McCarty NA (2013) Two salt bridges differentially contribute to the maintenance of cystic fibrosis transmembrane conductance regulator (CFTR) channel function. J Biol Chem 288(28):20758–20767